Published in final edited form as:

Nature. 2019 August ; 572(7771): 655–659. doi:10.1038/s41586-019-1478-7.

Wnt and TGFβ coordinate growth and patterning to regulate size-dependent behavior

Christopher P. Arnold[1,2,†], **Blair W. Benham-Pyle**[1,†], **Jeffrey J. Lange**[1], **Christopher J. Wood**[1], **Alejandro Sánchez Alvarado**[1,2,*]

[1]Stowers Institute for Medical Research

[2]Howard Hughes Institute for Medical Research

Differential coordination of growth and patterning across metazoans gives rise to a diversity of sizes and shapes at tissue, organ, and organismal levels. While tissue size and tissue function can be interdependent[1-5], mechanisms coordinating size and function remain poorly understood. Planarians are regenerative flatworms that bi-directionally scale their adult body size[6,7] and asexually reproduce, via transverse fission, in a size-dependent manner[8-10]. This paradigm offers a robust context to address the gap in knowledge underlying the link between size and function. A novel planarian fission protocol revealed that progeny number and fission initiation frequency scale with parent size. Fission progeny size is fixed by previously unidentified mechanically vulnerable planes spaced at an absolute distance along the anterior-posterior (A/P) axis. An RNAi screen of A/P patterning genes uncovered TGFβ and Wnt signaling components as regulators of fission initiation frequency rather than fission plane position. Finally, inhibition of Wnt and TGFβ signaling during growth altered the patterning of mechanosensory neurons, a neural sub-population that is distributed in accordance with animal size and modulates fission behavior. Therefore, our study identifies a novel role for TGFβ and Wnt in regulating size-dependent behavior, uncovering an interdependence between patterning, growth, and neurological function.

The infrequency of planarian fission behavior has largely precluded its mechanistic dissection. However, recently optimized animal husbandry techniques augmented fission activity[11-12], permitting us to study the integration of animal size with fission behavior. Large planaria from recirculation culture exhibited robust and reproducible increases in fission activity when transitioned to static culture and starved (Fig. 1a, Video S1). Live imaging provided detailed characterization of the fission process. Planarians first elongate and adhere their posterior tissue to a substrate. Next, periodic body contractions concentrate body mass towards the head region while thinning out tissues immediately anterior to the adherent tail. After 20-40 minutes, progressive stretching ruptures connecting tissue with

*Correspondence to: asa@stowers.org.

Authors contributions: Conceptualization, data analysis, and interpretation (CPA, BWBP, ASA), acquisition of data (CPA, BWBP, JJL), design and fabrication of planarian live imaging systems (JJL), software (CJW), data curation (JJL, CJW), writing of the original manuscript (CPA, BWBP), supervision and funding acquisition (ASA), and revision and editing of the manuscript (all authors).

†Authors contributed equally to this work

Competing Interests: The authors declare no competing interests.

rapid recoil, separating anterior parent and posterior fission progeny (Video S1, Extended Data Fig. 1a).

Observation of fission behavior in animals of increasing size showed that 1st posterior fission fragment length did not scale with parent length (Fig. 1b, d). Instead, larger animals produced additional progeny, each ~1mm in length, such that number of progeny after 2 weeks linearly correlated with parent size (Fig. 1c, e, Extended Data Fig 1. b-d). Thus, fission fragment size is fixed independent of A/P position or parent length. The frequency of fission fragment production – fission rate – did scale with animal length (Extended Data Fig. 1e, f) and both the time to 1st fission and time between sequential fission events was inversely related to parent size (Extended Data Fig. 1g-l). Automated webcam imaging of individual animals allowed us to generate timelines chronicling successful (upward displacement) and un-successful (downward displacement) fission attempts (Fig. 1f, Video S2). Fission attempts only occured in animals above 4-5mm in length, indicating a minimal size required for fission (Fig. 1g, h, Extended Data Fig. 2a, b). Furthermore, larger animals produced fission progeny more frequently due to more fission attempts (Fig. 1h, Extended Data Fig. 2 c, d), rather than higher rates of success (Fig. 1i). Altogether, these results confirm that planarian fission is a size-dependent behavior, with both progeny number and fission rate coupled to parent size.

We tested the hypothesis that patterning cues are required to coordinate animal size and planarian fission. Genes from the Wnt[13-16], TGFβ[17-19], and Hh[20] signaling pathways that regulate A/P identity were screened using RNA-dependent genetic interference (RNAi)[21] (Fig. 2a, b, Extended Data Fig. 3a, b). Re-screening confirmed 6 presumptive activators of fission (*ActR-1, smad2/3, β-catenin, Dsh-B, tsh, wnt11-6*) and a presumptive inhibitor (*APC*) (Fig. 2c). Parent animals morphology was observed at days 0 and 14 of the fission assay and in regenerating tissue fragments. RNAi knockdown reproduced published A/P patterning defects in regenerating tissue fragments (Extended Data Fig. 4a), but few morphological defects were observed in parent animals (Fig. 2d). On day 0, *β-catenin* RNAi animals exhibited morphological abnormalities while other RNAi conditions were indistinguishable from controls. By day 14, RNAi of *ActR-1* and *smad2/3* elicited motility defects, but RNAi of *Dsh-B*, *wnt11-6*, *tsh*, and *APC* significantly altered fission rate without changes in morphology. In situ staining of the CNS, intestine, and muscle confirmed published A/P polarity regeneration phenotypes, but no gross morphological defects in parent RNAi animals (Extended Data Fig. 4b-d). Therefore, we conclude that Wnt and TGF-β signaling components modulate fission behavior independent of overt body plan re-polarization.

Serendipitously, we discovered that compression of planaria reveals cryptic mechanically vulnerable planes that divide the animal at regularly spaced intervals along the A/P axis (Fig. 3a, b, Video S3. The number of these ‘compression planes’ scaled with animal size (Fig. 3b, c) and their position along the A/P axis overlapped with the position of fission planes (Fig. 3d). Furthermore, incomplete fission formed tears similar to those observed with compression (Extended Data Fig. 5a). Therefore, we conclude that compression planes are fission planes revealed by mechanical compression. Fission plane number and distribution correlated with animal length during tissue re-scaling and regeneration. Following

starvation, animals reduced body length and lost fission planes to restore number and distribution (Extended Data Fig. 5b-d). To assay fission plane regeneration, we amputated animals around the pharynx such that 90% of fragments contained a single plane (Extended Data Fig.5e-g). One week after amputation, animals remodeled, doubled in length, and increased fission plane number (Extended Data Fig.5f-j). Subsequent feeding increased animal length and fission plane number (Extended Data Fig.5f-j). Absent feeding, animals exhibited little to no elongation or plane addition despite re-scaling and regenerating their other tissues (Extended Data Fig.5f-j). In summary, fission planes are pre-established in planarians and scale dynamically with animal size and form.

Given the role of Wnt and TGFβ signaling in body patterning, we tested whether these genes regulate fission planes. RNAi-treated animals were mechanically compressed and the quantity and relative distribution of fission planes was measured (Fig. 3e-g). Surprisingly, while RNAi of *ActR-1* and *smad2/3* moderately reduced the number of fission planes, RNAi of Wnt signaling components had no effect on fission plane number or position (Fig. 3e, g, Extendended data Fig. 6a). Even knockdown of *wnt11-6* through 3 rounds of amputation/ regeneration failed to alter fission plane patterning (Figure 3f, g, Extendended data Fig. 6b). Hypomorphic RNAi knockdown of *β-catenin*, *ActR-1*, or *smad2/3* revealed little or no effect on fission fragment size (Extended Data Fig. 6c-e), further supporting the conclusion that neither Wnt nor TGF-β signaling regulate fission behavior through the A/P patterning of fission planes.

We tested whether Wnt and TGF-β signaling instread regulated the frequency of fission attempts. Using the automated webcam image capture system (Fig. 1f), we recorded fission behavior in RNAi-treated animals (Figure 4a). Remarkably, RNAi of *β-catenin*, *ActR*-1, *smad2/3*, and *wnt11-6* reduced fission attempts, while RNAi of *APC* increased fission attempts (Fig. 4b-d, Extended Data Fig. 7a-l, Video S5, Video S6). RNAi of *β-catenin* and *smad2/3*, which resulted in observable morphological abnormalities, also significantly reduced fission success ratio (Fig. 2d, 4e, Extended Data Fig. 7k-n). *Dsh-B* RNAi reduced the fission success ratio without altering the number or frequency of fission attempts (Fig. 4d, e, Extended Data Fig. 7k-n). Finally, *APC* RNAi reduced the time between fission attempts by ~50%, and animals initiated fission attempts independent of remaining tissue, dramatically reducing their success ratio (Fig. 4e, Extended Data Fig. 7i-n, Video S6). These findings demonstrate that Wnt and TGFβ signaling regulate the frequency of fission behavior.

We hypothesized that Wnt and TGFβ signaling components might regulate fisison behavior through the planarian central nervous system (CNS). Double fluorescent *in situ* hybridization (FISH) with the CNS marker *PC2* confirmed that Wnt and TGFβ fission regulators were detected in *PC2*+ cells in the anterior CNS (Extended Data Fig. 8a, b). Removal of anterior tissue containing the cephalic ganglia delayed the onset of fission behavior. (Extended Data Fig. 8c-f). Restoration of fission activity coincided with regeneration and re-establishment of anterior, *PC2* co-localized, *tsh* expression (Extended Data Fig. 8g). Surprisingly, removal of anterior tissue containing just one cephalic ganglion did not alter total fissions produced (Extended Data Fig. 8c-f), indicating that half of the CNS is sufficient to initiate fission. Finally, RNAi against *coe*, a transcription factor essential

for the patterning of the CNS[22,23], dramatically reduced planarian fission (Extended Data Fig. 8h, i). Altogether, these data support a model in which an anterior CNS expressing Wnt and TGFβ signaling components regulates fission initiation.

We hypothesized that polarity genes could modulate size-dependent behavior via size-dependent patterning of the CNS. To identify neuronal sub-populations regulating fission downstream of Wnt and TGFβ, we analyzed 17 neuronal markers[24-29] in small, medium, and large planaria and 10 markers in *smad2/3* RNAi treated animals (Fig 4f, Extended Data Fig 9a, b). Patterning of *pkd1L-2*$^{+}$, *gabrg3L-2*$^{+}$, and *sargasso-1*$^{+}$ mechanosensory neurons exhibited the clearest changes in both animals of increasing size and following *smad2/3* RNAi treatment (Extended Data Fig 9a, b). In large animals, mechanosensory neurons are tightly restricted to the anterior and knockdown of either *smad2/3* or *wnt11-6* broadened their distribution akin to that of smaller animal (Fig 4g-l). RNAi against *pkd1L-2* and *gabrg3L-2* (homologous to cation and chloride channel genes, respectively) increased planarian fission activity (Fig 4m, n) and live imaging of *gabrg3L-2* RNAi animals confirmed an increase in fission attempts without a reduction in fission success (Fig 4o-p, Extended Data Fig. 10, Video S7). These results indicate that mechanosensory neurons are differentially patterned during growth, inhibit fission behavior, and require Wnt and TGFβ for their appropriate patterning in accordance with animal size. Therefore, we conclude that Wnt and TGFβ signaling coordinates animal size and behavior via size-dependent patterning in the adult CNS.

In conclusion, we used planaria as a model for the integration of size, patterning, and function and established fission as a robust, reproducible, and quantifiable size-dependent behavior (Fig. 1, Video S1). While previous studies have generated physical models for the process of transverse fission[9], mechanisms coupling animal size and fission frequency have remained unknown. We discovered two independent mechanisms by which fission is coordinated with animal size in *Schmidtea mediterranea*. First, previously undescribed iterative structures patterned in accordance with A/P axis length couple animal size with the number of fission progeny produced (Fig. 3, Video S3). Second, the Wnt and TGFβ signaling pathways mediate size-dependent patterning of mechanosensory neurons, which regulate fission frequency (Fig. 4, Extended Data Fig. 9, 10). Thus, we demonstrate that differential patterning of key cell populations in accordance with tissue size provides a mechanistic link between animal growth and the acquisition or modulation of tissue function. Altogether, our results identify a novel role for Wnt and TGFβ patterning genes in regulating size-dependent behavior and show that developmental patterning cues coordinate tissue growth with size-dependent functions.

Methods

Animal Husbandry

Clonal CIW4 *Schmidtea mediterranea* were maintained in 1X Montjuic salts as previously described. CIW4 animals were sourced from a large recirculation culture as previously reported [11]. In brief, animals are housed in three culture trays (96’ L × 24’ W × 12’ H) stacked vertically. Water is recirculated through the system by a sump pump, which moves water through a chiller, a canister filter, a UV sterilizer, and the three housing trays. Water is

then passed through two vertically stacked sieves and a set of filter/floss pads before being returned to the sump pump. Animals were pulled from this system and either placed directly into fission assays, starved for at least 7 days prior to tissue fixation for imaging, or transferred to a unidirectional flow system culture for controlled feeding or RNAi feeding experiments.

Gene cloning and RNAi Feeding protocol

Candidate genes analyzed in this study were cloned from a CIW4 cDNA library into a pPR-T4P vector as described (Supplemental Table 1) [20]. These served as template for in vitro dsRNA synthesis for RNAi feedings. *Unc22* dsRNA was used for control RNA treatment. RNAi food was prepared by mixing 1 volume of dsRNA at 1600 ng/ml with 1.5 volumes of beef liver paste. For RNAi experiments targeting neuronal genes, 1 volume of dsRNA at 1400ng/ul was mized with 1 volume beef liver paste. The amount of food administered was 10ul of food per 1mm of worm length present in the worm flow container. Worms were allowed to feed for 6 to 10 hours with 2 rounds of light stimulation to facilitate additional consumption. Worms were fed every three days for a total of 3 RNAi feedings, unless otherwise specified. After RNAi feedings, worms were transferred to the relevant biological assay.

Fission Assay

A detailed protocol for fission induction has been made available through Protocol Exchange[10]. To induce fission, animals were removed from re-circulation culture or unidirectional flow system culture and washed 5-10 times with fresh 1X Montjuic salts. Individual animals were placed in 15cm tissue culture dishes with 50mL 1X Montjuic salts and their body length was measured. Representative images of d0 parents were captured using a Leica M205 microscope. Plates were stacked 6-12 dishes high and placed in a dark incubator at 20ºC. Daily, plates were removed from the incubator and fission fragments for each animal were counted and removed from the 15cm dish. For some experiments, images of fission fragments were taken on the day they were collected to allow for quantitation of fission fragment length. The 1X Montjuic salts in each individual dish was replaced weekly.

For data analysis, the number of daily cumulative fissions were divided by initial body length and then normalized to the average of the control RNAi fissions. This normalized fission score for each day was converted to a heat color code. Daily scores for each individual worm were aligned in descending order along the y-axis and the average score of each column was calculated and used to sort individual worms in ascending order along the x-axis. The average fission score of each RNAi condition was then sorted in ascending order from left to right. This resulted in a heat map visualization ranking the effects of RNAi treatments on fission activity.

Fission Plane Compression Assay

Fission planes were revealed by compression between a plastic tissue culture dish and a glass coverslip (See Video S3). Animals were inverted with their ventral side up, compressed using four fingertips, then imaged. To ensure that all compression/fission planes were revealed for every animal, images were acquired sequentially using a Leica M205

microscope as each fission plane was revealed by mechanical compression. Position of fission planes and distance between fission planes was quantified using Fiji (https://fiji.sc/). Video depicting compression assay was captured with an iPhone 6 (Apple).

Fluorescent whole mount *in situ* hybridization (FISH)

For RNA expression analyses, fluorescent in situ hybridization was performed as previously described[30,31]. Antibodies were used in MABT containing 5% horse serum for FISH (Roche anti-DIG-POD 1:1000 and Roche anti-FLCN-POD 1:1000) or NBT/BCIP in situ hybridization (Roche anti-DIG-AP 1:1000). For double FISH, peroxidase activity was quenched between tyramide reactions using 100mM sodium azide for at least 1 hour at room temperature with agitation. Nuclear staining was performed using 1:1000 Hoescht 33342 (Invitrogen) in PBSTx (1X PBS with 0.5% Triton-X-100).

Microscopy

Images of live worms and regenerating fission fragments were acquired using a Leica M205 microscope. Confocal images were acquired on an LSM-700-Vis and stitching was performed in Fiji using built-in grid collection plugins.

Live Imaging of Fission Behavior

Videos of worms from two orthogonal views were acquired using 2 webcams (Logitech C910/920). Webcams were mounted using a variety of ring stands and test tube clamps. The imaging chamber was a clear plastic square lid obtained from a box of coverslips. Lighting of the chamber was achieved using a Volpi illuminator (NCL-150). Each camera was connected to its own computer running micro-manager (https://micro-manager.org/). The cameras were set-up in micro-manager using OpenCVgrabber to set the pixel density (1920×1080) and to acquire the images. The camera gain, exposure and all other settings were set using the Logitech Webcam Controller software (https://download01.logi.com/web/ftp/pub/video/lws/lws280.exe) Data was acquired using the Multi-Dimensional Acquisition mode of micro-manager. The two computers were synchronized for acquisition manually at the beginning of the experiment.

For the high-throughput screening of fission behavior, worms were placed in 6 well dishes with cameras mounted above the plates using optics components (Thor Labs). Illumination was obtained using 4 LED ring lights (AmScope) mounted upside down and above the cameras to provide diffuse light. Image acquisition was performed using two different camera configurations: four cameras connected to one computer via a USB hub or one 4K camera connected to a USB port. In the four-camera configuration, images where captured sequentially from the cameras every 10 minutes. A script written in Python 3.6 (https://www.python.org/) was used as a wrapper for FFMPEG (https://www.ffmpeg.org/) to acquire images. The size of the images (1920×1080) and the pixel format (yuv420p) were set in the python script. The camera gain, exposure, and other settings where controlled with the Logitech Webcam Controller software (https://download01.logi.com/web/ftp/pub/video/lws/lws280.exe). The DirectShow framework was used to interface between the cameras and FFMPEG. In the single 4k camera setup, a 4096×2160 pixel image was captured every ten

minutes from a Logitech BRIO webcam. The same python script was used as a wrapper for FFMPEG in this configuration.

Quantification of Live Imaging

Videos of individual animals were manually annotated. For each fission attempt the start time and completion time were recorded and the success or failure of the attempt was recorded. To depict fission behavior, a timeline was constructed and a numerical value was given to each frame of a video. A value of 0 was assigned to any frame in which no fission behavior was observed, a positive value was given to any frame during a successful fission attempt, and a negative value was given to any frame during a failed fission attempt (see Fig. 1f). A prolonged diagonal line in a timeline indicates a period where frames were not acquired due to failed communication between the image acquisition software and the webcam.

Statistical Tests

For all pair-wise comparisons, significance was tested using an un-paired Student t-test. GraphPad Prism was used to calculate Pearson correlation coefficients with a two-tailed 95% confidence interval and to perform linear regression analyses. Two-way ANOVA analysis was performed in Graphpad Prism to determine the significance or RNAi treatment over time.

Data Availability Statement:

Source data and construct sequences can be accessed from the Stowers Original Data Repository at http://www.stowers.org/research/publications/libpb-1356. All other data are available from the corresponding author upon reasonable request

Code Availability Statement:

Code for the Python 3.6 (https://www.python.org/) script used for a wrapper for FFMPEG (https://www.ffmpeg.org/) for the high-throughput recording of fission behavior is available at the Stowers Original Data Repository at http://www.stowers.org/research/publications/libpb-1356.

Extended Data

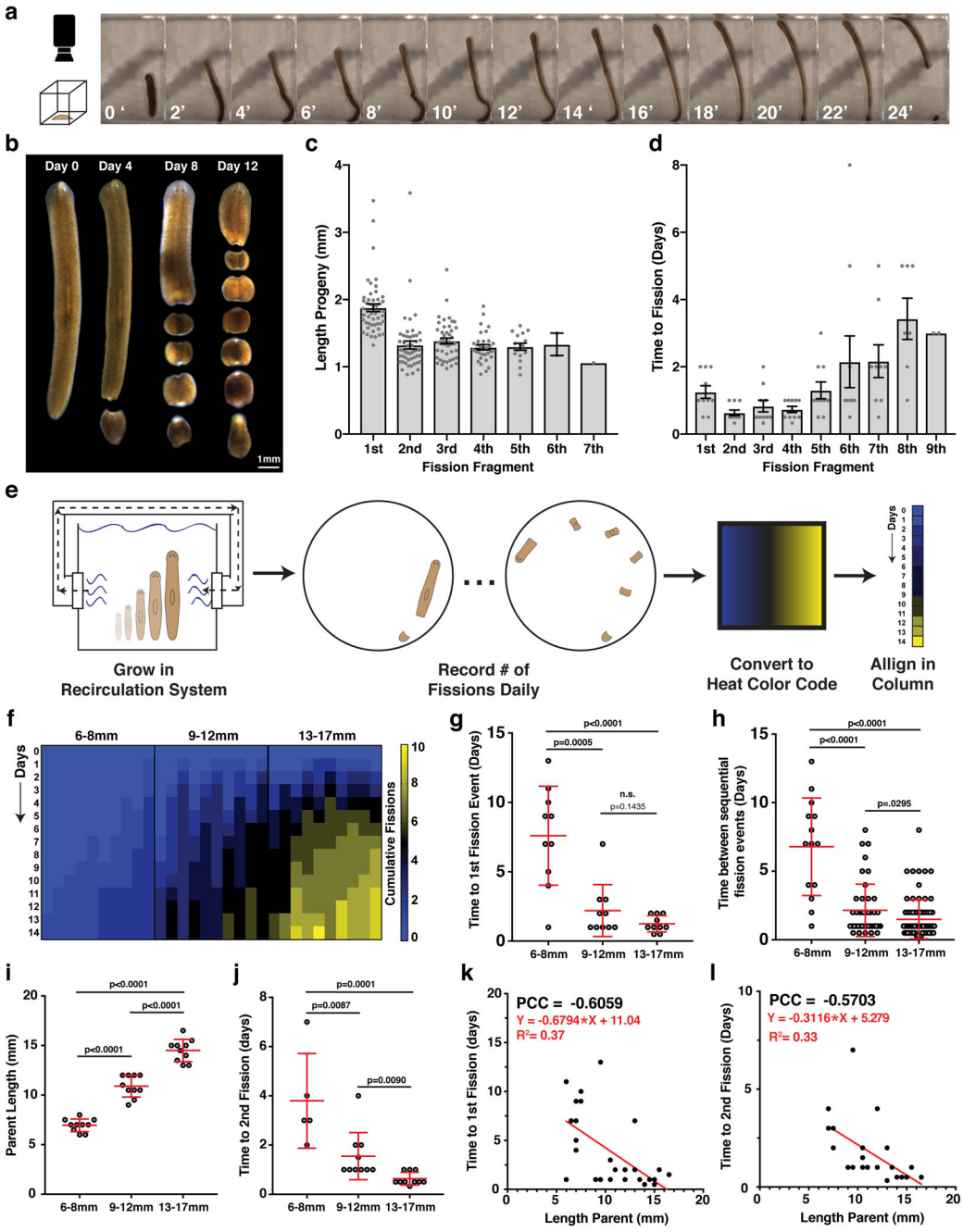

Extended Data Fig. 1: Characterization of planarian fission biology.

a, Live imaging of large planarian worm during fission (representative of 12 experiments, see also Video 1). **b,** Imaging of single individual large planarian and regenerating progeny 0, 4, 8, and 12 days after fission induction (experiment repeated 50 times). **c, d,** A/P length of progeny and time to fission event since induction or previous fission (mean, SEM, n=50 animals). Fission fragments binned by position along the A/P axis (1st fission = most posterior). **e,** Schematic representation of fission induction and quantitative scoring system used to compare fission activity between different conditions. **f,** Cumulative fission fragments produced over 14 days by individual animals binned by parent size (n=10 per

bin). **g, h,** Time to first fission event or time between sequential fission events for animals 6-8mm, 9-12mm, or 13-17mm in length. **i,** Raw parent length measurement of planarian individuals 6-8mm, 9-12mm, or 13-17mm in length. **j,** Time between 1st and 2nd fission events for animals 6-8mm, 9-12mm, or 13-17mm in length (mean, SEM, n= 139 independent measurements from 30 animals). **k, l,** Time between induction and first fission or between 1st and 2nd fission plotted relative to parent length, with Pearson correlation co-efficient, linear regression, and R^2 value (n= 26 and 21 independent measurements from 30 animals). Statistics determined by two-sided t-test.

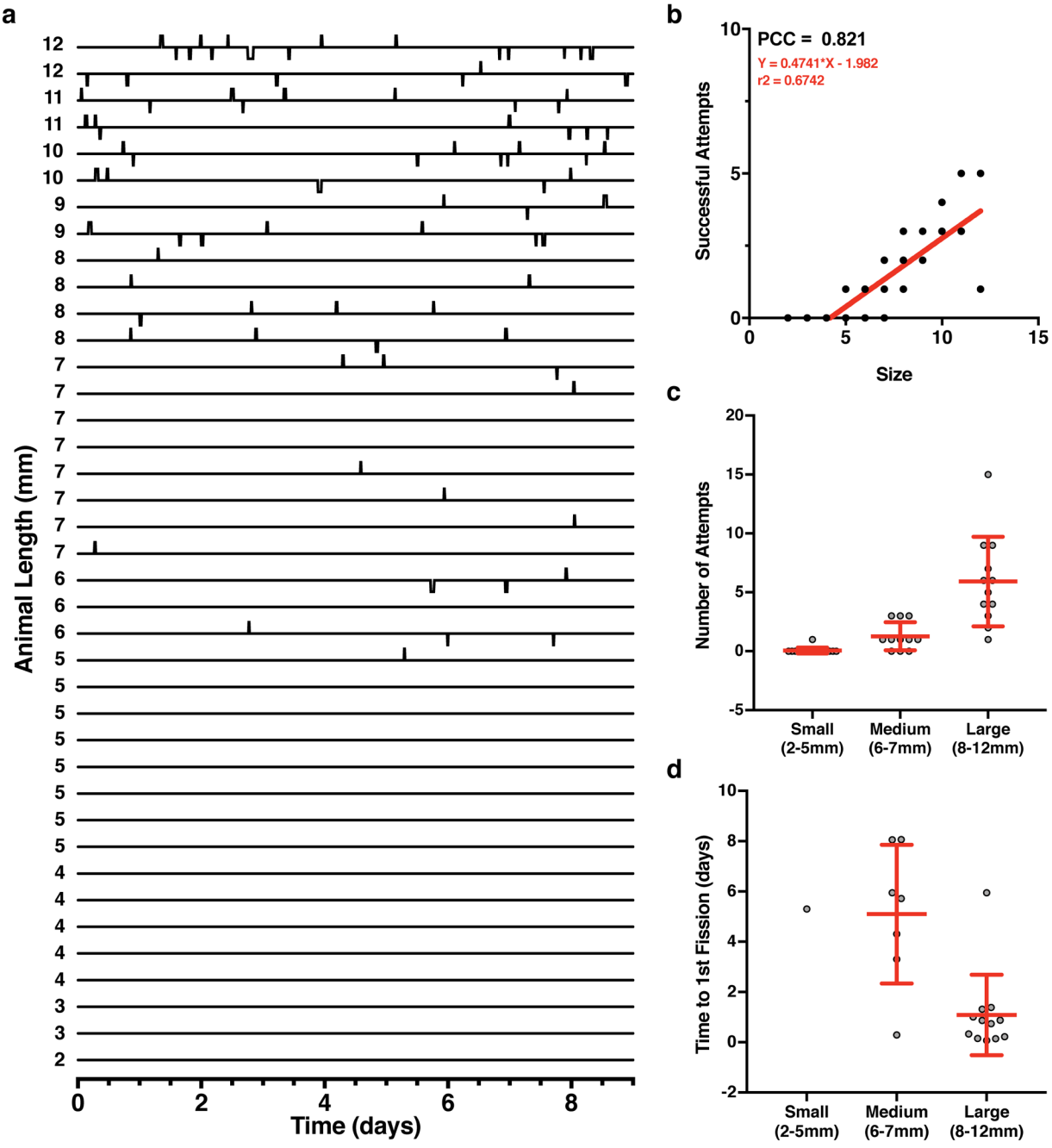

Extended Data Fig. 2: Quantitation of fission behavior across a range of animal sizes.

a, All individual timelines depicting fission activity over 9 days for animals ranging from 2mm (bottom) to 12mm (top) in length (n=39 animals). **b,** Number of successful fission attempts per animal relative to parent length. **c, d,** Number of fission attempts and time to 1st fission attempt for animals binned into small (2-5mm), medium (6-7mm), and large (8-12mm) groups (mean, SEM, n=16 small, 11 medium, 12 large animals).

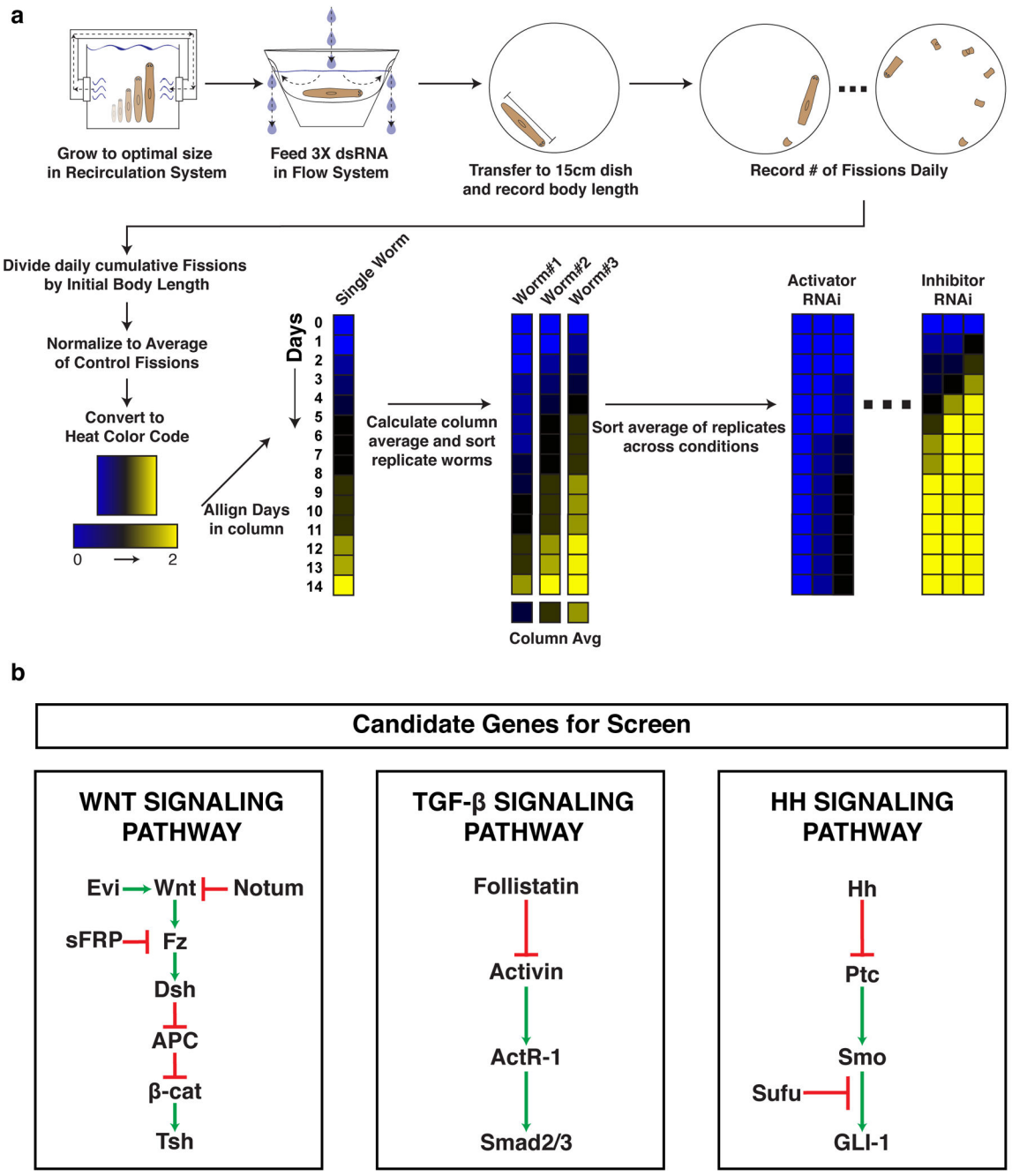

Extended Data Fig.3: Strategy for a targeted RNAi screen to identify regulators of fission.

a, Detailed schematic of RNAi workflow. Animals are grown to an optimal size in the recirculation culture system and transferred to a flow system for RNAi feedings. After 3 RNAi feedings, worms were transferred to a 15cm dish and animal length recorded. The number of fissions were recorded daily for 14 days for each worm from each RNAi condition. For data analysis, the number of daily cumulative fissions were divided by initial body length and then normalized to the average of the control RNAi fissions. For data visualization, this normalized fission score for each day was converted to a heat color code. Daily scores for each individual worm were aligned in ascending order along the y-axis. The

average score of each column is calculated and used to sort individual worms in ascending order along the x-axis. The average fission score of each RNAi condition was then sorted in ascending order from left to right. The result is a heat-map visualization ranking the effects of RNAi treatments on fission activity. **b,** Wnt, TGF-β, Hh signaling pathway diagrams focusing on components targeted for RNAi screen. Green arrows indicate positive interaction and red arrows indicate inhibitory interaction.

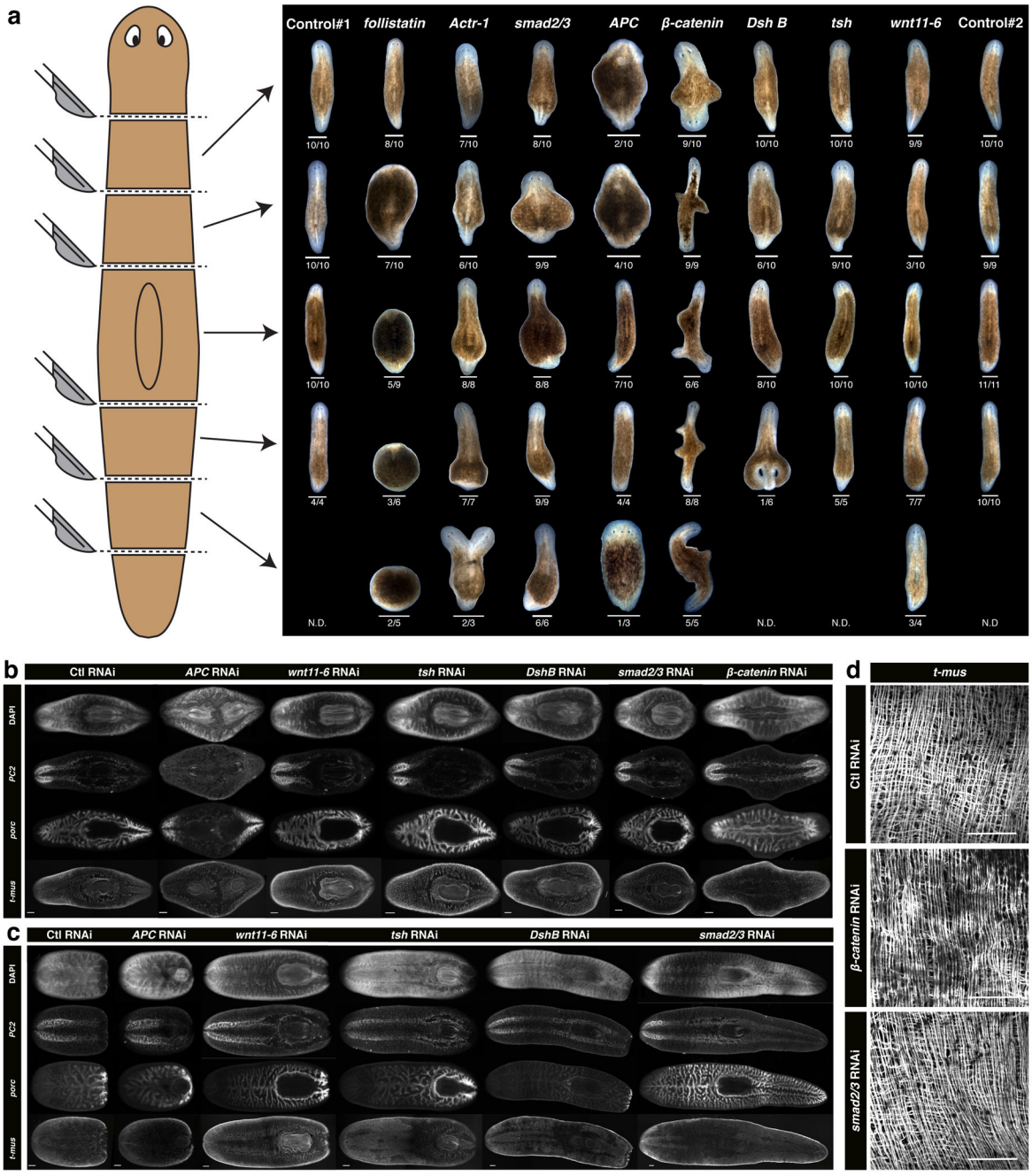

Extended Data Fig. 4: Analysis of morphology and/or internal tissues in regenerating fragments and fissioning parents.

a, Representative images of regenerating tissue fragments from different positions along the A/P axis at 15 days post amputation (dpa). Fraction of animals with pictured phenotype along with 1mm scale bar depicted below each image. **b, c,** In situ staining of CNS (*PC2*), intestine (*porc*) and muscle (t-mus) tissues at (**b**) day 15 of regeneration or (**c**) the fission assay. **d,** High resolution image of body wall musculature (t-mus) in control RNAi and *smad2/3* or *β-catenin* RNAi treated animals. Representative images (n=7-13 animals). All

images are oriented ventral side up with anterior on the left side. (Experiment performed a single time. Scale, 0.5mm)

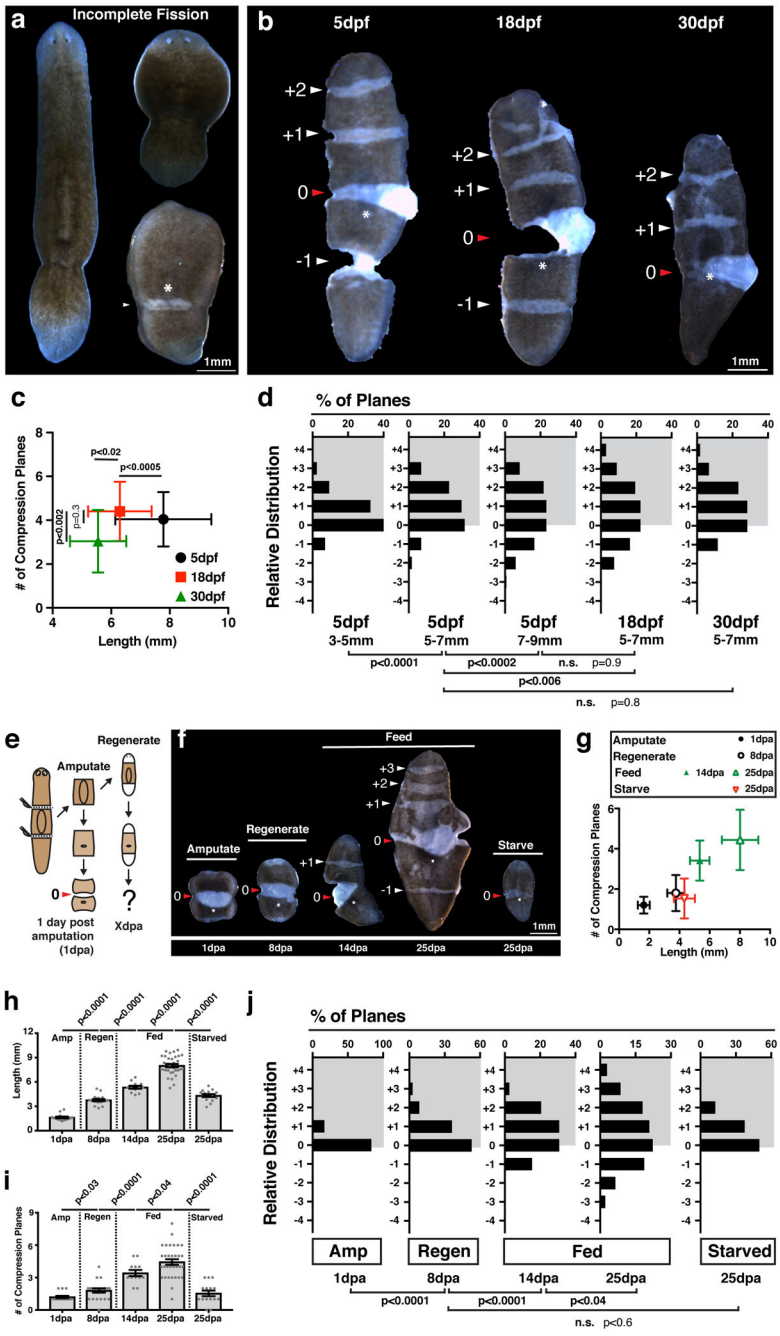

Extended Data Fig. 5: Effects of Growth, Starvation, and Regeneration on fission planes.

a, Image of planaria after incomplete fission, revealing ventral tear identical to compression planes (observed greater than 5 independent times). **b,** Post-compression worms at 5dpf, 18dpf and 30dpf (5dpf image from same experiment as Fig. 3b; single experiment).**c, d,** Bidirectional plot (**c**) of compression planes versus animal length (n=25, mean, SD), and relative distribution (**d**) of planes at 5dpf, 18dpf, or 30dpf (n=28, 18, 31, 15, and 19 animals). **e,** Schematic of experiment tracking establishment of fission planes during tissue regeneration. **f, g,** Representative images and bidirectional plot of compression planes versus

animal length (mean, SD) following amputation (1dpa, n=15 animals), regeneration (8dpa, n=19 animals), and growth (Fed 14dpa and 25dpa, n= 12 and 32 animals) or de-growth (Starved 25dpa, n=15 animals) (single experiment). **h-j,** Graph of (**h**) animal length, (**i**) # of compression planes (mean, SEM), and (**j**) relative distribution of planes following amputation (1dpa, n=15 animals), regeneration (8dpa, n=19 animals), and growth (Fed 14dpa and 25dpa, n= 12 and 32 animals) or de-growth (Starved 25dpa, n=15 animals).

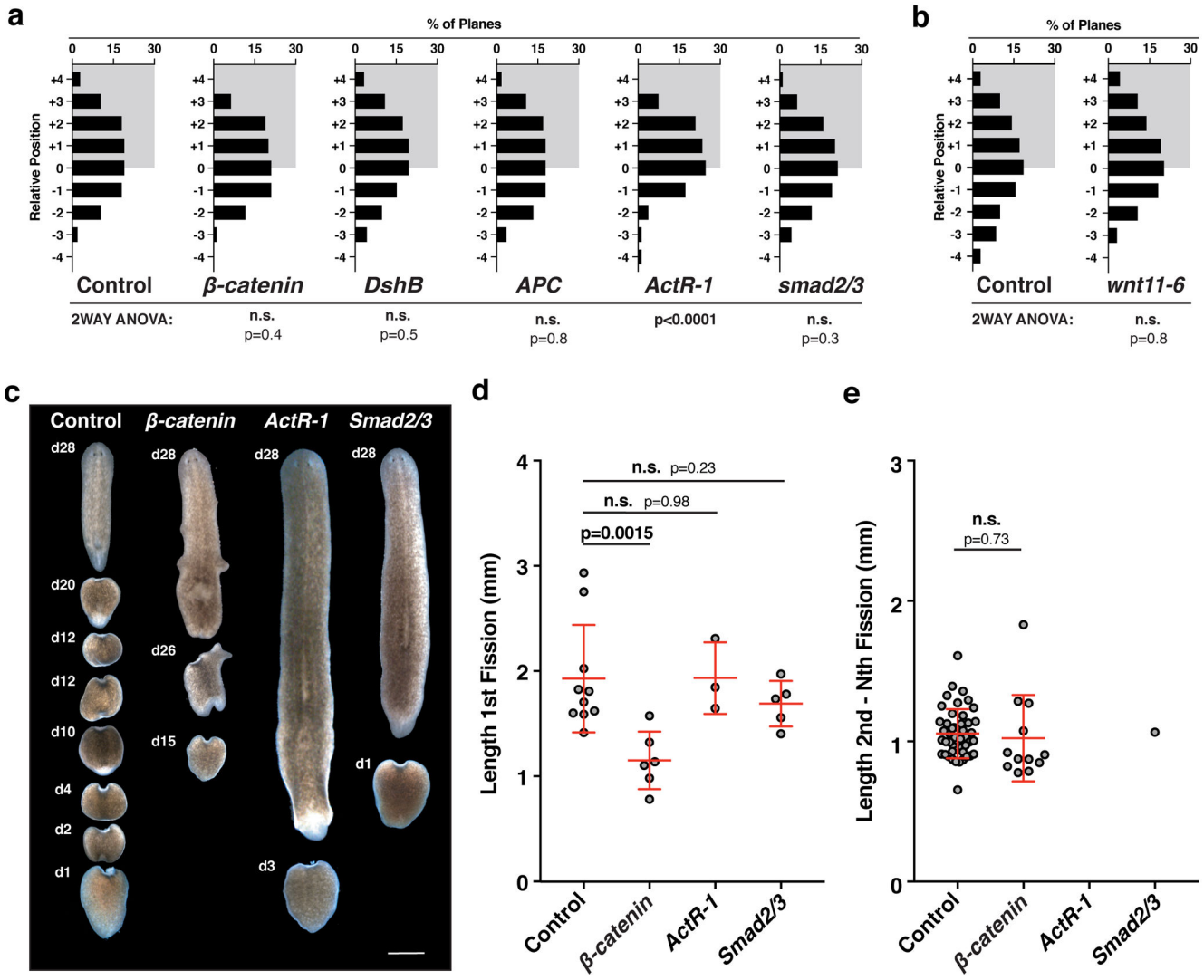

Extended Data Fig. 6: Effects of Wnt/TGF-β signaling component RNAi on fission planes.

a, b, Relative plane distribution following RNAi treatment (n=20 and 10 animals). **c,** representative images of progeny within 24 hours of fission and of remaining parent tissue at day 28 after fission induction for animals treated with control, *β-catenin*, *ActR-1*, or *smad2/3* RNAi. (experimentally independently performed twice. Scale, 1mm). **d, e,** Length of the first fission progeny or all subsequent progeny in animals treated with control, *β-catenin*, *ActR-1*, or *smad2/3* RNAi (mean, SEM, n= 85 fission fragments from 36 animals). p-value calculated with 2-way ANOVA Interaction Factor (**a, b**) or two-sided t-test (**d, e**).

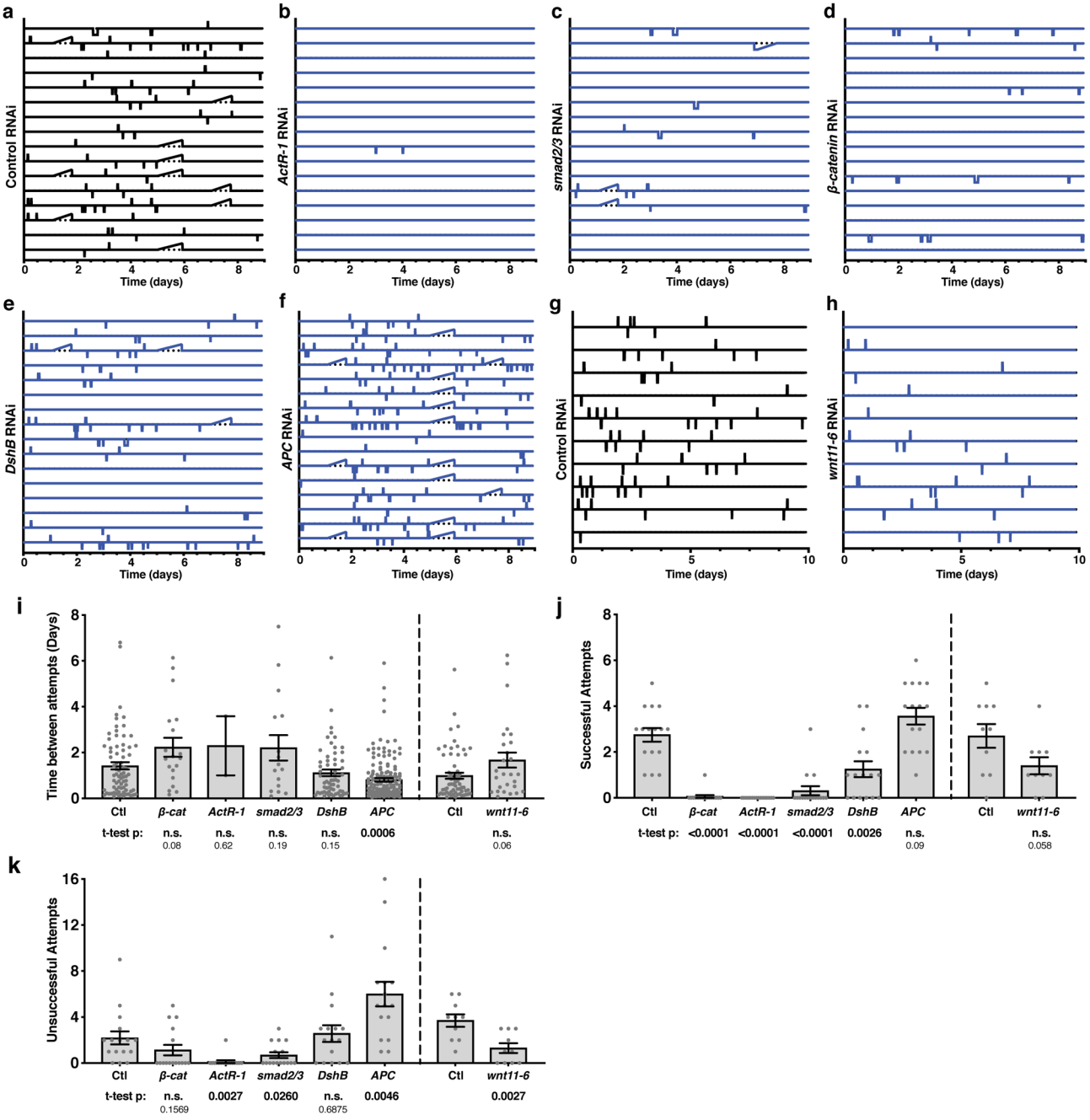

Extended Data Fig. 7: Wnt and TGFβ signaling components regulate the frequency of fission initiation.1

a-h, All individual timelines depicting fission activity over 9-10 days for animals treated with (**a,g**) Control, (**b**) *ActR-1*, (**c**) *smad2/3*, (**d**) *β-catenin*, (**e**) *DshB*, (**f**) *APC*, or (**h**) *wnt11-6* RNAi. **i-n,** Graphs depicting (**i, j**) the time between sequential fission attempt, (**k, l**) the number of successful fission attempts, (**m,n**) the number of unsuccessful fission attempts in animals fed dsRNA targeting fission regulators (mean, SEM, n= 421 fission events from 116 animals). Animals were given either 3 (**a-f, i, k, m**) or 18 (**g,h,j,l,n**) dsRNA feedings. Batched experiments are plotted separately. p-value calculated with two-sided t-test.

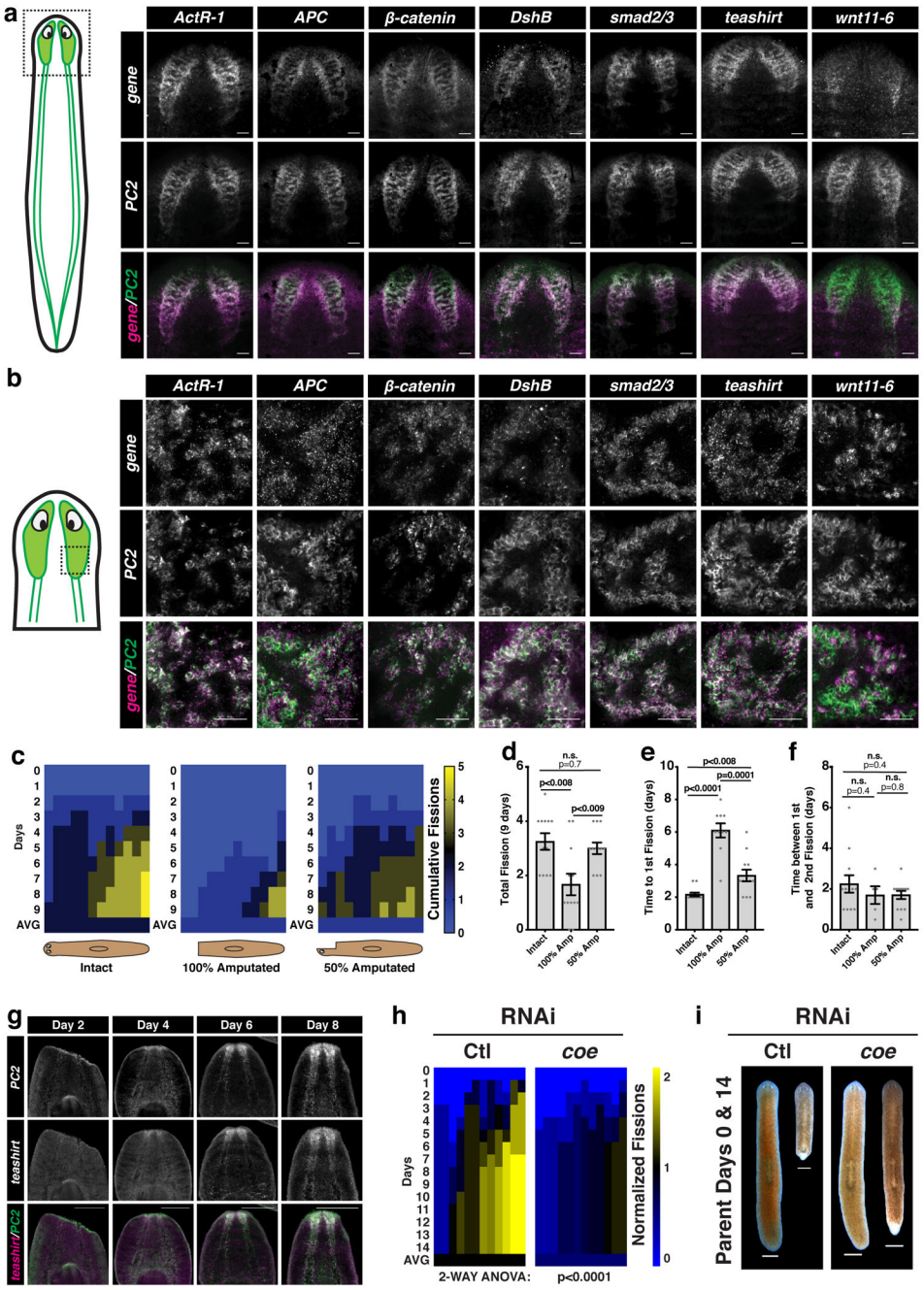

Extended Data Fig. 8: The planarian anterior CNS regulates fission.

a, Whole brain imaging of *PC2* and fission regulator gene expression detected by double fluorescent *in situ* hybridization (n=2-4 animals; experiment independently repeated; Scale, 100**μ**m). **b,** Single cell co-expression of *PC2* and fission regulators in the posterior branches of the anterior CNS. (n= 3-5 animals; Scale bar, 50**μ**m) (n=3-5). **c,** Fission induction in intact, 100% head amputated, or 50% head amputated animals over a 9-day observation period (n=12 animals). **d-f**, Plot of (**d**) total number of fission progeny over 9 days, (**e**) time between fission induction and 1st fission, (**f**) and time between 1st and 2nd fission for intact, 100% head amputated, or 50% head amputated animals (mean, SEM, n= 94 fission events

from 36 animals). **g,** Regeneration time course in 100% head amputated animals showing recovery of anterior gene expression of *PC-2* co-localized with *teashirt*. (n=4-5 animals; experiment performed a single time; Scale, 500**μ**m). **h,** Heatmaps depicting fission activity following *coe* RNAi treatment. Normalized cumulative fissions over time are displayed for individual worms from each RNAi condition (n=12 animals). **i,** Representative parent images on days 0 and 14 of the fission assay (n=12, experiment independently performed twice; Scale, 1mm). p-value calculated with two-sided t-test (**d-f**) or 2-WAY ANOVA (**h**).

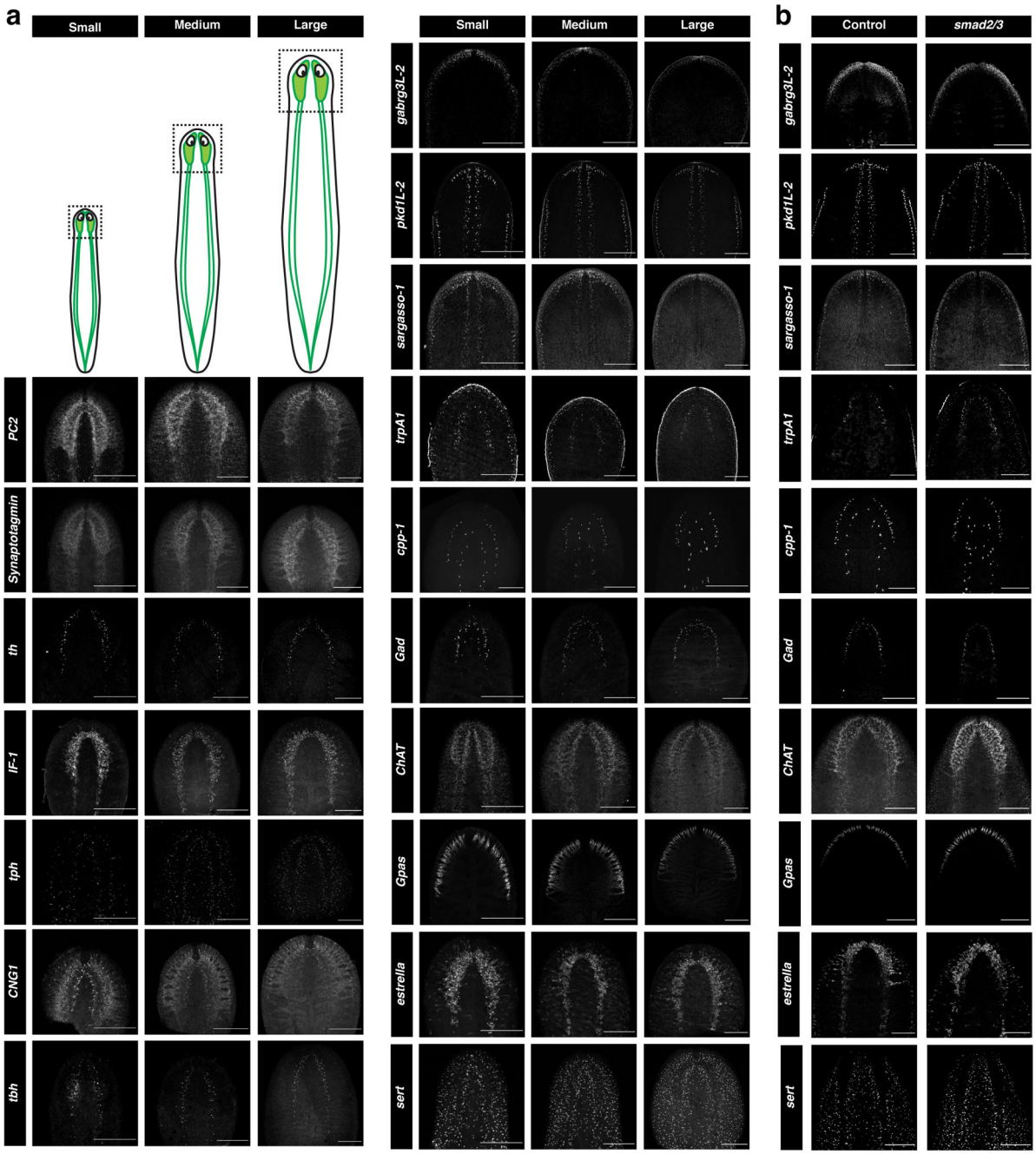

Extended Data Fig. 9: Comparison of neuronal subpopulations in animals of increasing size and following *smad2/3* RNAi treatment

a, Representative images of neuronal marker staining in small, medium and large animals (n=3-5 animals; 1 experiment). **b,** Representative images of a subset of neuronal markers analyzed in *smad2/3* RNAi-treated animals (n=3-5 animals; 1 experiment). Scale, 0.5mm.

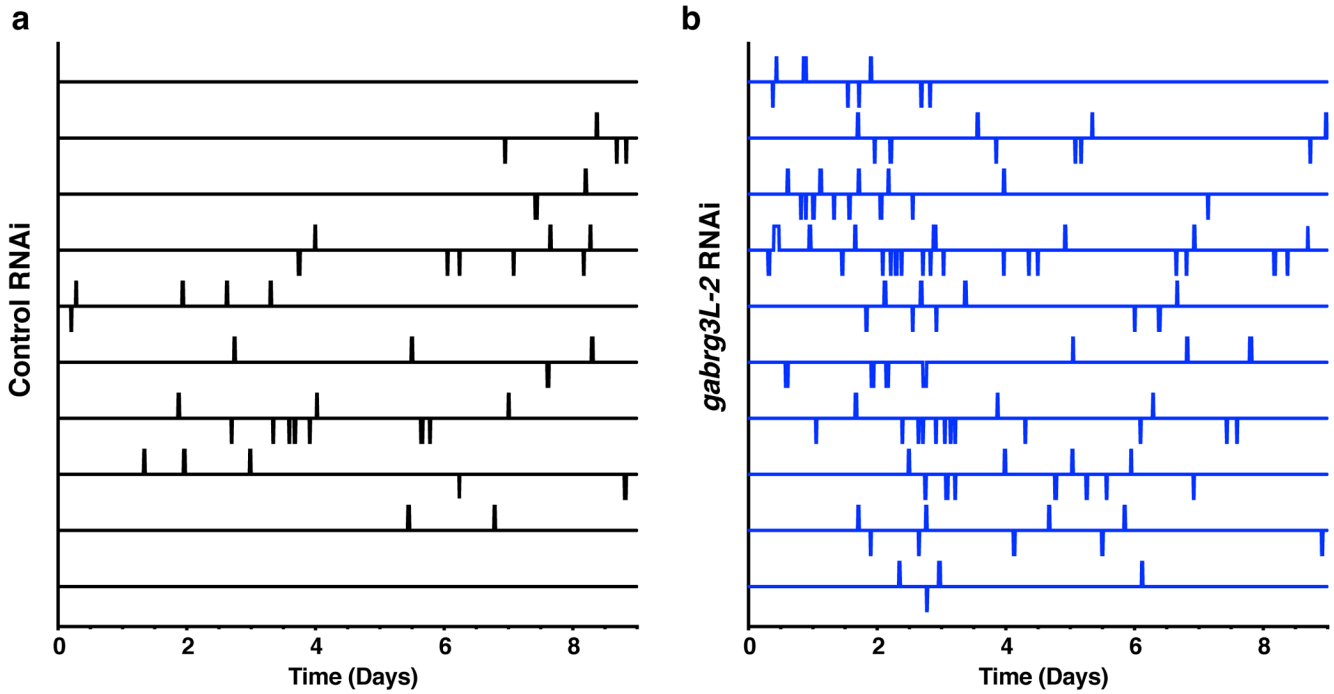

Extended Data Fig. 10: *Gabrg3L-2* negatively regulates the frequency of fission initiation.
a-b, All individual timelines depicting fission activity over 9 days for animals treated with (**a)** Control or (**b**) *gabrg3L-2 RNAi* (n=recordings of 10 animals combined from two independent experiments).

Supplementary Material

Refer to Web version on PubMed Central for supplementary material.

Acknowledgements:

We thank members of the ASA laboratory for discussion and advice, Frederick Mann for providing unpublished reagents, and Kausik Si for comments. We are grateful to the Stowers Planarian and Microscopy core facilities for technical contributions and methods development.

Funding: ASA is a Howard Hughes Medical Institute (HHMI) and Stowers Institute for Medical Research Investigator. BWBP is a Jane Coffin Childs Memorial Fund Postdoctoral Fellow. CPA is a HHMI Postdoctoral Fellow. This work was supported in part by NIH R37GM057260 to ASA.

References:

1. Rinkevich Y, Montoro DT, Contreras-Trujillo H, Harari-Steinberg O, Newman AM, Tsai JM, Lim X, Van-Amerongen R, Bowman A, Januszyk M, Pleniceanu O, Nusse R, Longaker MT, Weissman IL, Dekel B, In vivo clonal analysis reveals lineage-restricted progenitor characteristics in mammalian kidney development, maintenance, and regeneration, Cell Rep 7, 1270–1283 (2014). [PubMed: 24835991]
2. Kaufman JM, Siegel NJ, Hayslett JP, Functional and hemodynamic adaptation to progressive renal ablation, Circ. Res. 36, 286–293 (1975). [PubMed: 1116239]
3. Fleming S, Thompson M, Stevens R, Heneghan C, Plüddemann A, Maconochie I, Tarassenko L, Mant D, Normal ranges of heart rate and respiratory rate in children from birth to 18 years of age: a systematic review of observational studies, The Lancet 377, 1011–1018 (2011).

4. Bryant PJ, Simpson P, Intrinsic and extrinsic control of growth in developing organs, The Quarterly review of biology 59, 387–415 (1984). [PubMed: 6393189]
5. Hafen E, Stocker H, How Are the Sizes of Cells, Organs, and Bodies Controlled? PLoS Biol 1, e86 (2003). [PubMed: 14691557]
6. Oviedo NJ, Newmark PA, Sánchez Alvarado A, Allometric scaling and proportion regulation in the freshwater planarian *Schmidtea mediterranea*, Developmental Dynamics : an official publication of the American Association of Anatomists 226, 326–333 (2003). [PubMed: 12557210]
7. Stuckemann T, Cleland JP, Werner S, Thi-Kim Vu H, Bayersdorf R, Liu S-Y, Friedrich B, Julicher F, Rink JC, Antagonistic Self-Organizing Patterning Systems Control Maintenance and Regeneration of the Anteroposterior Axis in Planarians, Dev Cell 40, 248–263.e4 (2017). [PubMed: 28171748]
8. Best JB, Goodman AB, Pigon A, Fissioning in planarians: control by the brain, Science 164, 565–566 (1969). [PubMed: 5778008]
9. Malinowski PT, Cochet-Escartin O, Kaj KJ, Ronan E, Groisman A, Diamond PH, Collins E-MS, Mechanics dictate where and how freshwater planarians fission, Proc Natl Acad Sci USA, 201700762 (2017).
10. Thomas MA, Quinodoz S, Schotz E-M, Size Matters! J Stat Phys 148, 664–676 (2012).
11. Arnold CP et al. Pathogenic shifts in endogenous microbiota impede tissue regeneration via distinct activation of TAK1/MKK/p38. eLife 5, (2016).
12. Arnold Christopher, Benham-Pyle Blair, Sánchez Alvarado Alejandro. Planarian Fission Induction Protocol. Protocol Exchange (2019) DOI: 10.21203/rs.2.10324/v1.
13. Gurley KA, Rink JC, Sánchez Alvarado A, Beta-catenin defines head versus tail identity during planarian regeneration and homeostasis, Science 319, 323–327 (2008). [PubMed: 18063757]
14. Roberts-Galbraith RH, Newmark PA, Follistatin antagonizes activin signaling and acts with notum to direct planarian head regeneration, Proc Natl Acad Sci U S A 110, 1363–1368 (2013). [PubMed: 23297191]
15. Hill EM, Petersen CP, Wnt/Notum spatial feedback inhibition controls neoblast differentiation to regulate reversible growth of the planarian brain, Development 142, 4217–4229 (2015). [PubMed: 26525673]
16. Petersen CP, Reddien PW, Wnt signaling and the polarity of the primary body axis, Cell 139, 1056–1068 (2009). [PubMed: 20005801]
17. Reddien PW, Bermange AL, Kicza AM, Sánchez Alvarado A, BMP signaling regulates the dorsal planarian midline and is needed for asymmetric regeneration, Development 134, 4043–4051 (2007). [PubMed: 17942485]
18. Gavino MA, Reddien PW, A Bmp/Admp regulatory circuit controls maintenance and regeneration of dorsal-ventral polarity in planarians, Curr Biol 21, 294–299 (2011). [PubMed: 21295483]
19. Molina MD, Saló E, Cebrià F, The BMP pathway is essential for re-specification and maintenance of the dorsoventral axis in regenerating and intact planarians, Dev Biol 311, 79–94 (2007). [PubMed: 17905225]
20. Rink JC, Gurley KA, Elliott SA, Sánchez Alvarado A, Planarian Hh signaling regulates regeneration polarity and links Hh pathway evolution to cilia, Science 326, 1406–1410 (2009). [PubMed: 19933103]
21. Sánchez Alvarado A, Newmark PA, Double-stranded RNA specifically disrupts gene expression during planarian regeneration, Proc Natl Acad Sci U S A 96, 5049–5054 (1999). [PubMed: 10220416]
22. Cowles MW, Brown DDR, Nisperos SV, Stanley BN, Pearson BJ, Zayas RM, Genome-wide analysis of the bHLH gene family in planarians identifies factors required for adult neurogenesis and neuronal regeneration, Development, 140, 4691–4702 (2013). [PubMed: 24173799]
23. Cowles MW, Omuro KC, Stanley BN, Quintanilla C/G, Zayas RM, COE loss-of-function analysis reveals a genetic program underlying maintenance and regeneration of the nervous system in planarians, PLoS Gen, 10, e1004746 (2014).
24. Wenemoser D, Lapan SW, Wilkinson AW, Bell GW, Reddien PW, A molecular wound response program associated with regeneration initiation in planarians, Genes Dev, 26, 988–1002 (2012). [PubMed: 22549959]

25. Arenas OM, Zaharieva EE, Para A, Vasquez-Doorman C, Petersen CP, Gallio M, Activation of planarian TRPA1 by reactive oxygen species reveals a conserved mechanism for animal nociception, Genesis 53, 1686–1693 (2017).

26. Currie KW and Pearson BJ, Transcription factors lhx1/5-1 and pitx are required for the maintenance and regeneration of serotonergic neurons in planarians, Development, 140, 3577–3588 (2013). [PubMed: 23903188]

27. Collins JJ III, Hou X, Romanova EV, Lambrus BG, Miller CM, Saberi A, Sweedler JV, Newmark PA, Genome-wide analyses reveal a role for peptide hormones in planarian germline development, PLoS Biol, 8, e1000509 (2010) [PubMed: 20967238]

28. Roberts-Galbraith RH, Brubacher JL, Newmark PA, A functional genomics screen in planarians reveals regulators of whole-brain regeneration, eLife, 5, e17002 (2016). [PubMed: 27612384]

29. Ross KG, Molinaro AM, Romero C, Dockter B, Cable KL, Gonzalez K, Zhang S, Collins EMS, Pearson BJ, Zayas RM, SoxB1 activity regulates sensory neuron regeneration, maintenance, and function in planarians, Dev Cell, 47, 331–347.e5 (2018). [PubMed: 30399335]

30. Pearson BJ et al. Formaldehyde-based whole-mount in situ hybridization method for planarians. Developmental Dynamics : an official publication of the American Association of Anatomists 238, 443–450 (2009). [PubMed: 19161223]

31. King RS & Newmark PA In situ hybridization protocol for enhanced detection of gene expression in the planarian Schmidtea mediterranea. BMC Dev Biol 13, 8 (2013). [PubMed: 23497040]

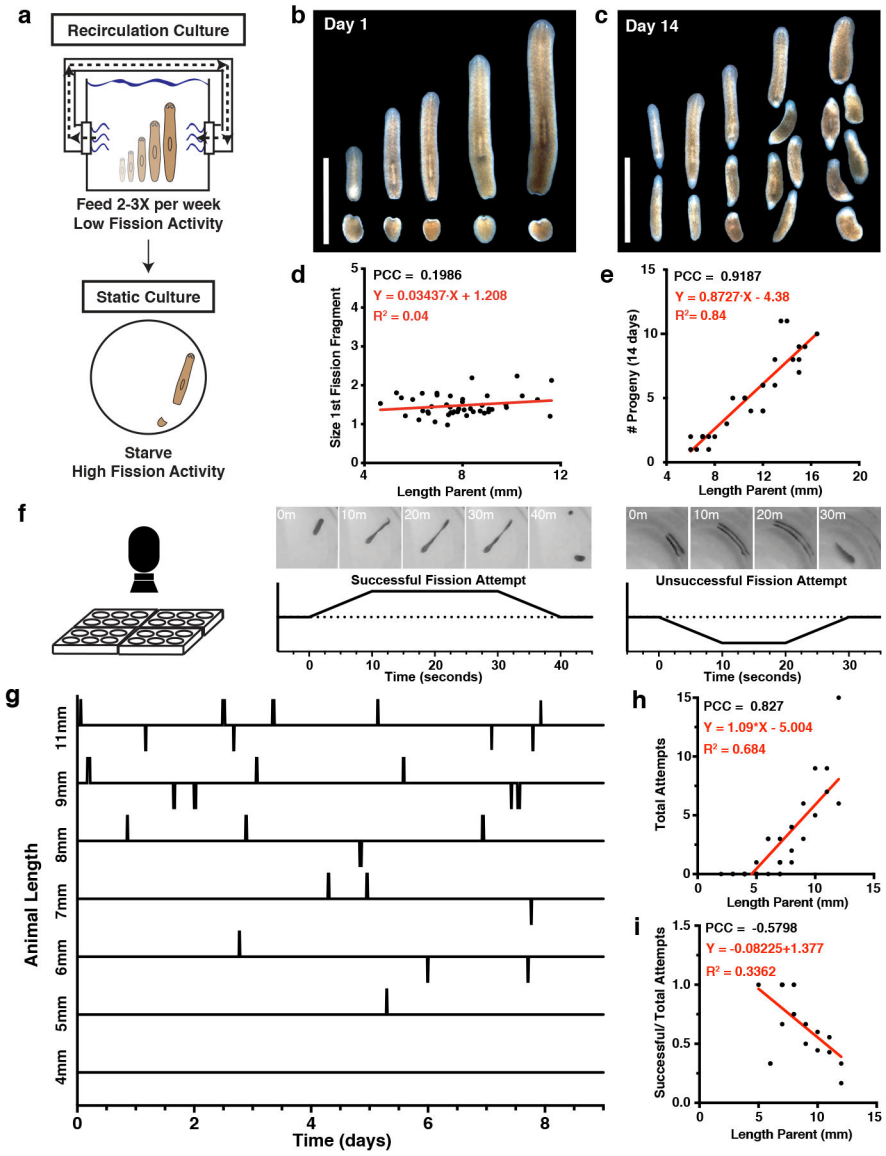

Fig.1: Planarian fission is a size-dependent behavior.

a, Optimized fission protocol. **b, c,** Representative images of 5-12mm animals (scale, 5mm) and fission fragments (**b**) <24 hours and (**c**) 14 days after first fission (n = 46 animals from 1 experiment). **d,e,** First fission fragment length and progeny number over 2 weeks relative to parent length (n=46 (d) or 30 (e) animals from 1 experiment). **f,** Webcam live imaging schematic (left) and example timeline graphing successful (middle) versus unsuccessful (right) fission attempts. **g,** Representative fission behavior timelines from a range of parent lengths. **h, i,** Total fission attempts and successful attempts/total attempts relative to parent length (n=39 or 21 animals, single experiment). Pearson Correlation Co-efficient (PCC), linear regression (red line), and R^2 value provided for scatter plots.

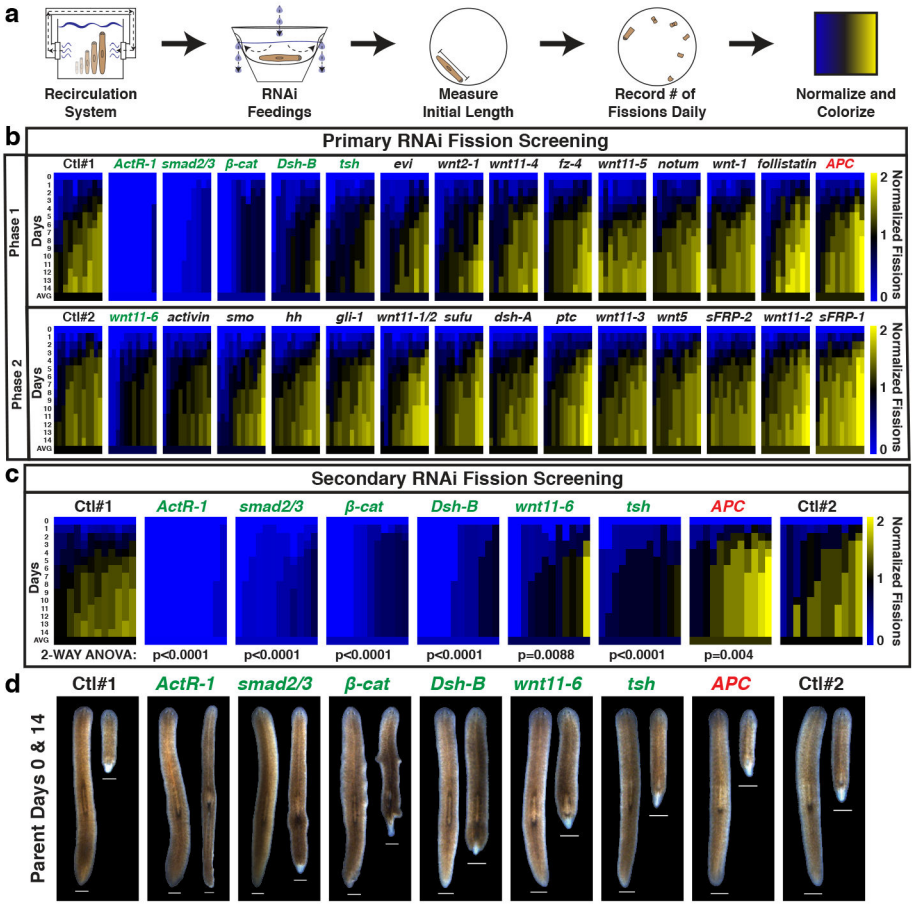

Fig. 2: Wnt signaling and TGF-β signaling components modulate fission activity.

a, RNAi Screen Workflow (See also Extended Data Fig. 3). **b, c,** Heatmaps depicting fission activity following RNAi treatment for both the (**b**) 2-phase primary and (**c**) secondary RNAi screens. Normalized cumulative fissions over time are displayed for individual worms from each RNAi condition (n=10 animals for Phase I, n=12 animals for Phase II and Secondary Screen). Targets in secondary screening (independently repeated 3 times) depicted in green (activators) and red (inhibitors). Significance determined by interaction factor of 2-way ANOVA. **d,** Representative parent images on days 0 and 14 of the fission assay (n= 10-12, independently repeated 3 times). Scale,1mm.

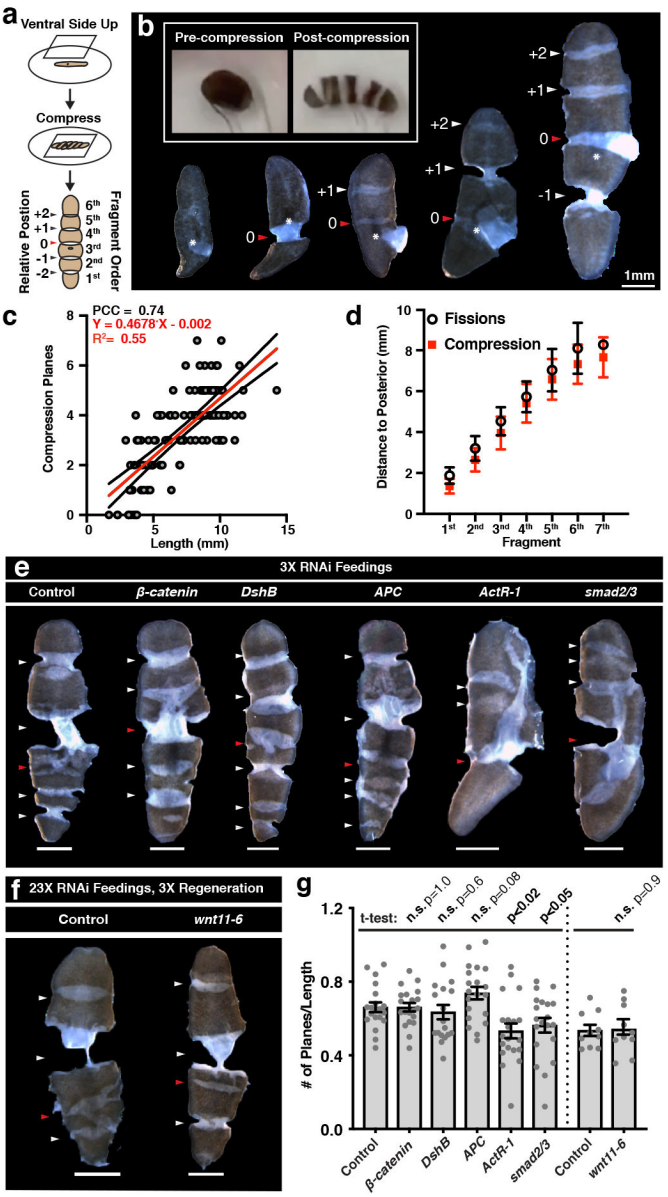

Fig. 3: Pre-established fission planes determine progeny size independent of Wnt/TGF-β signaling.

a, Schematic of compression assay, see Video S3. **b,** Pre- and post-compression worm (inset) and compression planes revealed in 3-6mm animals (independently repeated 5 times). **c,** Compression plane number relative to animal length (n=117 animals), with PCC, linear regression (red line), R^2 value, and 95% confidence interval (black lines). **d,** Fission (n=196 fission progeny from 50 animals) and compression plane (n=173 planes from 30 animals) overlap along the A/P axis of the animal (graph reports mean with error bars = SD). **e, f,** Representative images of post-compression animals following knockdown of Wnt and TGF-β signaling components using the specified number of RNAi feedings and rounds of regeneration (n depicted by dot plot quantification, experiment performed three times (e) or

once (f); Scale, 1mm) **g,** Plot of the number of fission planes/animals length following RNAi treatment (mean, SEM, n=20 and 10 animals). p-value calculated with two-sided t-test.

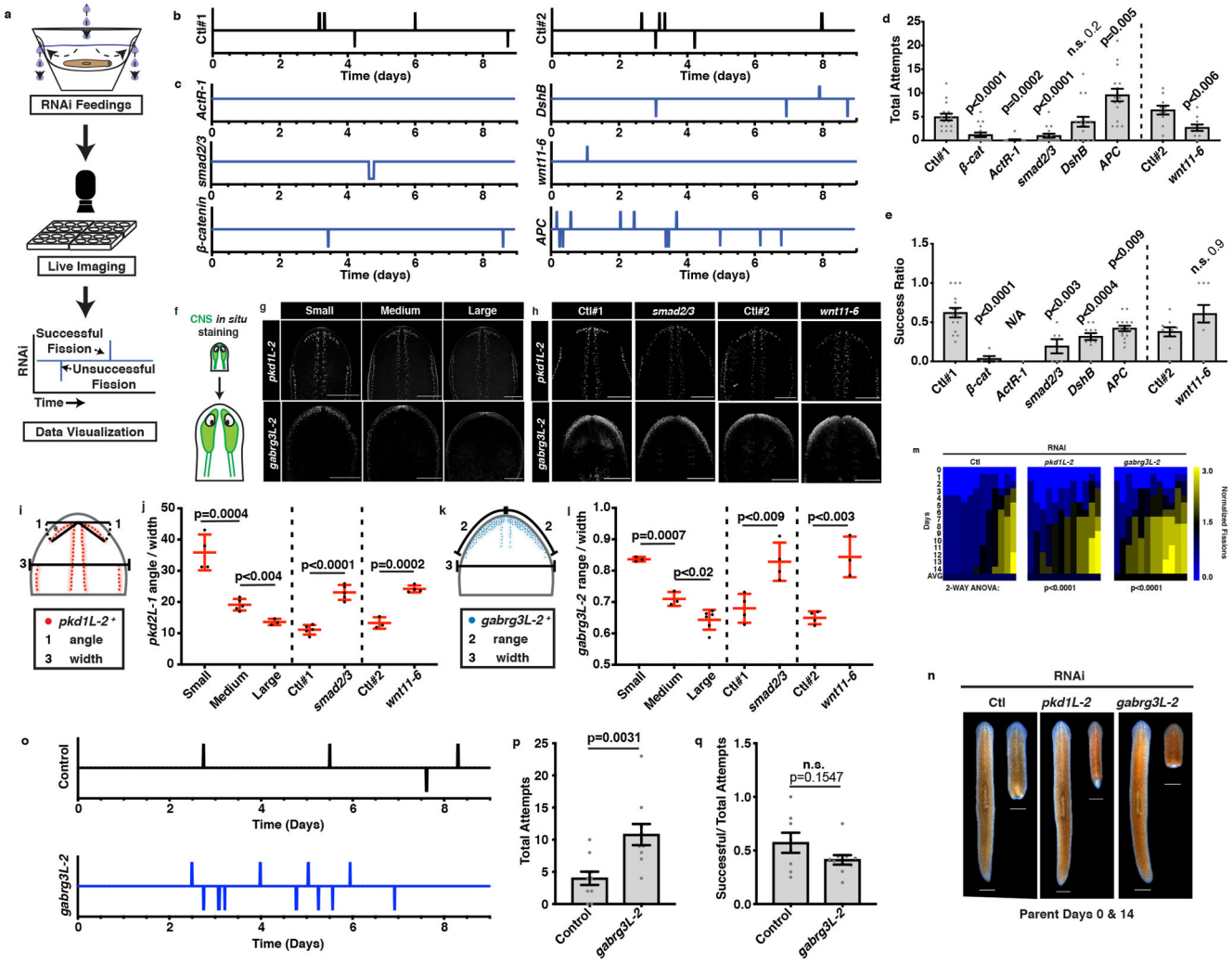

Fig. 4: Wnt/TGF-β signaling regulates fission frequency via size-dependent patterning of mechanosensory neurons in the CNS.

a, Schematic depicting RNAi treatment, live imaging, and data analysis **b, c,** Representative activity timelines **d, e,** Total fission attempts and successful attempts/total attempts for RNAi-treated animals (mean, SEM, n=16 animals, 10 animals, 1 to 2 independent experiments). **f,** Schematic depicting in situ staining strategy. **g, h,** Representative images of *pkd1L-2*$^{+}$ and *gabrg3L-2*$^{+}$ neurons in animals (**g**) of increasing size, or (**h**) following RNAi treatment. Scale, 0.5mm. **i, k**, Diagrams depicting quantification of (**i**) the angle of *pkd1L-2*+ cells or (**k**) the range of *gabrg3L-2*$^{+}$ cells. **j, l** *pkd1L-2* (**j**)and *gabrg3L-2* (**l**) staining quantification in animals of increasing size or following RNAi treatment. (mean, SEM, n=3-6, exact n depicted in dot plot quantification) **m,** Fission activity heatmaps following *pkd1L-2* and *gabrg3L-2* RNAi treatment (see also Figure 2, n=12). **n,** Representative parent images on days 0 and 14 of fission assay (n=12, two independent expeirments, Scale, 1mm). **o,** Representative fission activity timelines of *gabrg3L-2* RNAi-treated animals. **p, q,** Total fission attempts and proportion of successful out of total fission

attempts for *gabrg3L-2* RNAi-treated animals (mean, SEM, n=10 animals). Significance determined by two-sided t-test (**j, l, p, q**) or 2-way ANOVA